Alternating quantum-emitter chains: Exceptional-point phase transition, edge state, and quantum walks

Jimin Li[1] and Zongping Gong[2,3]
[1]*Institute of Physics, University of Bonn, Nussallee 12, 53115 Bonn, Germany*
[2]*Department of Applied Physics, University of Tokyo, 7-3-1 Hongo, Bunkyo-ku, Tokyo 113-8656, Japan*
[3]*Theoretical Quantum Physics Laboratory, Cluster for Pioneering Research, RIKEN, Wako-shi, Saitama 351-0198, Japan*

(Received 26 May 2023; accepted 7 February 2024; published 23 February 2024)

We study the long-range hopping limit of a one-dimensional array of N equal-distanced quantum emitters in free space, where the hopping amplitude of emitter excitation is proportional to the inverse of the distance and equals the lattice dimension. For two species of emitters in an alternating arrangement, the single excitation sector exhibits non-Hermitian spectral singularities known as exceptional points. We unveil an unconventional phase transition, dubbed *exceptional-point phase transition*, from the collective to individual spontaneous emission behaviors. At the transition point, the $N \times N$ Hamiltonian fragments into $N/2-1$ many two-dimensional nondiagonalizable blocks. The remaining diagonalizable block contains a dissipation-induced edge state with algebraically localized profiles, and we provide numerical evidence for its existence in the infinite-array limit. We demonstrate that the edge state can be eliminated via a continuous deformation, consistent with the ill-definedness of bulk topological invariant. We also propose a spatially resolved character to quantify the incoherent flow and loss in the nonunitary quantum walks of single atomic excitations.

DOI: 10.1103/PhysRevA.109.023718

I. INTRODUCTION

Structured arrays of quantum emitters, typically modeled as two-level atoms, have attracted much attention in the contexts of quantum technologies, photon storage, and nonlinear optics, owning the advantages of having controllable light-matter interfaces [1–6]. A main issue in improving the quantum protocols' efficiency is the phenomenon of spontaneous emission. In general cases, light couples to matter both coherently and dissipatively, causing photon leakage or reabsorbing into undesired optical modes. Recently, subradiant states of N atoms with $O(N^{-\alpha})$ decay rates were found in finite subwavelength atomic arrays in three-dimensional (3D) free space, known as the subradiance scaling [7–11]. Here, subwavelength means that the emitter spacing is smaller than the light wavelength corresponding to the atomic transition frequency. Under such conditions, the light-mediated interactions between emitters can be described by an effective non-Hermitian long-range Hamiltonian, known as the resonant dipole-dipole interaction (RDDI) [10].

Meanwhile, over the past years, the theoretical interests originated novel non-Hermitian phenomena such as the exceptional points (EPs) [12–14], skin effects [15,16], and non-Hermitian topology [17–19] in various open classical and quantum systems that have synchronized with controllable experimental setups in the platforms of atomic, molecular, and optical physics [20–24]. These phenomena arise from the unique complex spectral structures and nonorthogonality (or even incompleteness) of eigenstates without Hermitian counterparts. However, previous works mostly focus on short-range systems with finite hopping ranges. The interplay between non-Hermiticity and long-range interactions, which are the two fundamental features of subwavelength atomic arrays, remains largely unexplored.

In this work, we study the single excitation sector of subwavelength alternating atomic chains in 3D free space through the lens of non-Hermitian physics. In particular, we consider the hopping decay power equal to the lattice dimension, which is 1. This is a marginal value from the angle of thermodynamic stability [25,26]. When tuning the strength of alternation, we demonstrate this realistic model shows a non-Hermitian behavior which we call *exceptional-point phase transition*. At the transition point, the $N \times N$ Hamiltonian in the single excitation sector can be decomposed into $N/2-1$ many nondiagonalizable (Jordan) and one diagonalizable 2×2 blocks. Away from the transition point, the new dispersion relation modifies the RDDI subradiance scaling.

In addition, we numerically show the existence of an edge state with a power-law decaying tail under the dissipative long-range hopping, despite the fact that a bulk topological invariant is ill-defined. Lastly, we consider the real-time dynamics by investigating a spatially resolved escape distribution and wave-function density. We generalize the conventional character to account for not only on-site loss but also incoherent hopping. We find an initial quantum walker with parity symmetry shows an imbalance of escape rates and densities at the boundaries at late time. Our work provides a paradigm for exploring novel phases and dynamics in long-range non-Hermitian systems, for which naïve approximations such as dropping of non-Hermitian terms and truncation of long-range hopping may lead to qualitatively incorrect results.

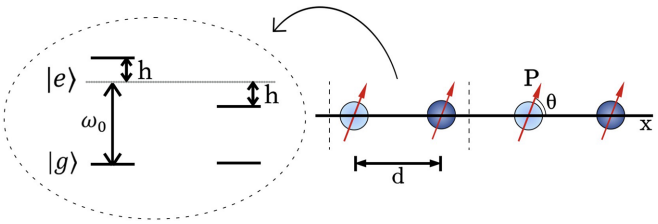

FIG. 1. Illustration of a 1D array of alternating quantum emitters in 3D free space; the two species have transition energies $\omega_0 \pm h$. The standard RDDI is recovered by setting identical transition energies, namely $h = 0$.

II. ONE-DIMENSIONAL ARRAY OF QUANTUM EMITTERS

We consider a one-dimensional (1D) array of N equal-distanced quantum emitters in 3D free space. Each emitter is a two-level atom with an internal structure of the ground $|g\rangle$ and excited state $|e\rangle$, separated by an atomic transition energy gap ω_0 (see in Fig. 1). For a subwavelength interatomic distance d, the collective spontaneous emission of atomic ensemble involves light-matter interactions between atoms and all the electromagnetic modes in free space. Welsch *et al.* have developed a generalized input-output formalism based on the classical 3D free-space electromagnetic Green's tensor $\mathbf{G}(\mathbf{r}_i, \mathbf{r}_j, \omega)$ to capture such collective effect, where $\mathbf{r}_i$ denotes the position of the ith atom [27–30]. The transition frequency ω_0 is typically much larger than other relevant energy scales, implying that optical responses have a narrow window around ω_0. Under the Born-Markov approximation $\mathbf{G}(\mathbf{r}_i, \mathbf{r}_j, \omega) \simeq \mathbf{G}(\mathbf{r}_i, \mathbf{r}_j, \omega_0)$, one can solve for the atomic degrees of freedom and obtain an effective light-field mediated long-range non-Hermitian Hamiltonian, i.e., the RDDI Hamiltonian

$$H_{\mathrm{RDDI}} = -\mu_0\omega_0^2 \sum_{i,j=1}^{N} \mathbf{P}^* \cdot \mathbf{G}(\mathbf{r}_i, \mathbf{r}_j, \omega_0) \cdot \mathbf{P}\, \sigma_i^\dagger \sigma_j, \qquad (1)$$

where μ_0 is the magnetic constant, $\sigma_i^\dagger = |e_i\rangle\langle g_i|$ excites the ith atom, $\mathbf{P}$ is the transition dipole, and $\mathbf{G}(\mathbf{r}_i, \mathbf{r}_j, \omega_0) = \mathbf{G}(\mathbf{r}_i - \mathbf{r}_j, \omega_0)$ with

$$\mathbf{G}(\mathbf{r}, \omega_0) = \frac{e^{ik_0 r}}{4\pi k_0^2 r^3}\Big[\big(k_0^2 r^2 + ik_0 r - 1\big)\mathbf{1} + \big(-k_0^2 r^2 - 3ik_0 r + 3\big)\frac{\mathbf{r}\otimes\mathbf{r}}{r^2}\Big], \qquad (2)$$

$k_0 = \omega_0/c$ is the wave number corresponding to the atomic transition energy, $r = |\mathbf{r}|$ (c: speed of light). Hereafter, we set the atomic spontaneous emission rate $\gamma_0 = \mu_0\omega_0^3|\mathbf{P}|^2/(3\pi\hbar c)$ to be the unit.

In the $N \to \infty$ infinite-array limit and under the assumption that the coordinate origin coincides with an atom, the single excitation sector of H_{RDDI} is diagonalized by the Bloch states

$$H_{\mathrm{RDDI}}(\sigma_{\mathbf{k}}^\dagger |\mathbf{g}\rangle) = \omega_{\mathrm{eff}}(\sigma_{\mathbf{k}}^\dagger |\mathbf{g}\rangle), \qquad (3)$$

where $|\mathbf{g}\rangle = |g\rangle^{\otimes N}$, $\sigma_{\mathbf{k}}^\dagger = \sum_{j=1}^{N} e^{i\mathbf{k}\cdot\mathbf{r}_j}\sigma_j^\dagger/\sqrt{N}$, and

$$\omega_{\mathrm{eff}} = -\frac{3\pi}{k_0}\hat{\mathbf{P}}^* \cdot \left[\sum_{j=1}^{N} e^{-i\mathbf{k}\cdot\mathbf{r}_j}\mathbf{G}(\mathbf{r}_j, \omega_0)\right] \cdot \hat{\mathbf{P}}$$

is the dispersion relation (here, $\hat{\mathbf{P}} = \mathbf{P}/|\mathbf{P}|$), which is determined from the Fourier-transformed Green's tensor [10]. The long-range hopping of the excitation forms a band that has the energy $\Re(\omega_{\mathrm{eff}})$ and decay rate $-2\Im(\omega_{\mathrm{eff}})$. Recalling that all the atoms are located on a line, which is chosen to be the x axis, we know that the perpendicular component of $\mathbf{k}$ does not alter the state or energy. Hence, it suffices to focus on $\mathbf{k} = k\hat{\mathbf{x}}$ with $k \in (-\pi/d, \pi/d]$. The Bloch states of $|k| > k_0$ are off-resonant and hence perfectly subradiant, namely, $\Im(\omega_{\mathrm{eff}}) = 0$.

Realistic experimental realizations of such a 1D array consist of only a finite number of atoms with an open boundary condition (OBC), which modifies the infinite chain results. The major effect is that all the off-resonant states gain a nonzero decay rate; starting from the lowest decay rate, the first ξ [$\xi \ll N$ is of $O(1)$] subradiant states show a $N^{-\alpha}$ scaling and recover a zero decay rate in the infinite-array limit.

A. Long-range hopping limit

In 1D atomic arrays, the hopping terms

$$G(r) = \mu_0\omega_0^2 \mathbf{P}^* \cdot \mathbf{G}(r\hat{\mathbf{x}}, \omega_0) \cdot \mathbf{P} \qquad (4)$$

of H_{RDDI} are in the following power-law forms [31]:

$$\Re[G(r)] \propto (1-\cos^2\theta)\frac{\cos(k_0 r)}{k_0 r} - (1-3\cos^2\theta)\left[\frac{\sin(k_0 r)}{(k_0 r)^2} + \frac{\cos(k_0 r)}{(k_0 r)^3}\right],$$

$$\Im[G(r)] \propto (1-\cos^2\theta)\frac{\sin(k_0 r)}{k_0 r} - (1-3\cos^2\theta)\left[\frac{\cos(k_0 r)}{(k_0 r)^2} - \frac{\sin(k_0 r)}{(k_0 r)^3}\right],$$

where the highest-power exponent can be r^{-1} or higher depending on the angle from dipole to the 1D array $\theta = \arccos(\hat{\mathbf{P}} \cdot \hat{\mathbf{x}})$. In this work, we focus on the long-range hopping limit of H_{RDDI} by setting $\theta = \arccos(1/\sqrt{3}) = 0.955$, where the power-law decay hopping exponent equals the spatial dimension and the resulting terms are simply proportional to the zeroth spherical Bessel functions.

In this work, the interatomic distance is fixed to be $k_0 d = \pi/2$ for reasons to be explained in the next section, as considered in Fig. 2 (upper panels, red), which shows the dispersion relation in the infinity chain limit, obtained by the discrete Fourier transform (FT) of the Green's function (4). The decay rate is given by the rectangle function, which is just the FT of $\sin(r)/r$. Thus, the collective decay rate is a constant for all $|k| < \pi/(2d)$ within the light line, discontinuous at the light line $|k| = \pi/(2d)$, and zero for $|k| > \pi/(2d)$, implying perfect subradiance. The real part of H_{RDDI} is proportional to $\cos(k_0 r)/(k_0 r)$, and its FT is ill-defined due to the singularity at $r = 0$.

The singular term at $r = 0$ has a divergent real part, known as the single-atom energy shift, which we set to zero without

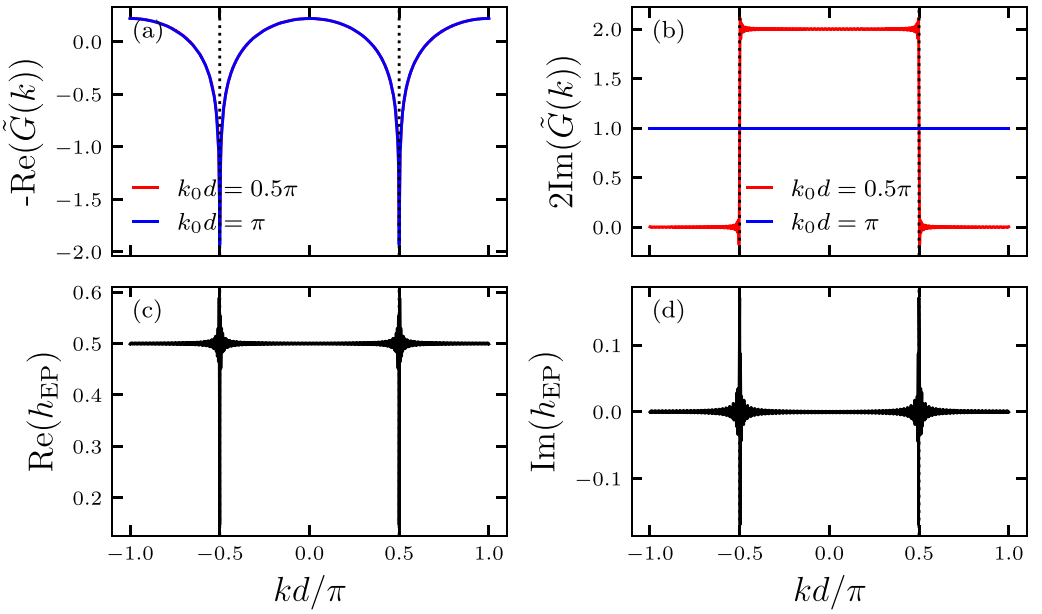

FIG. 2. (Upper (a) and (b)) The discrete Fourier transformed Green's function (5) in 1D at $k_0d = \pi/2$ (red) and $k_0d = \pi$ (blue) for the long-range hopping $\theta = \arccos(1/\sqrt{3})$. The imaginary part of the red curve is discontinuous at the light line, as shown in (b). (Lower (c) and (d))The infinite-array limit predictions of h_{EP} at $\theta = \arccos(1/\sqrt{3})$. h_{EP} equals 0.5 for states of all quasimomentum except the light line.

the loss of generality (in principle, it is absorbed into a renormalized transition energy ω_0). The imaginary part gives the vacuum atomic emission rate, and this constant term is added to all calculations throughout the text. For argument's sake, such diverging on-site potential is not explicitly written out here, and the discrete FT

$$\tilde{G}_d(k) = \sum_{n\in\mathbb{Z}\setminus\{0\}} e^{-ikdn} G(dn) \tag{5}$$

has no closed form.

A useful quantity to consider is the discrete Fourier transformed Green's function $\tilde{G}_{2d}(k)$ at another interatomic distance $k_0d = \pi$, which is the minimal interatomic distance for the absence of subradiance in 1D finite array, and the dispersion is shown in Fig. 2 (blue). We find the numerical values of the real dispersion are the same as $\Re[\tilde{G}_d(k)]$ up to negligible finite-size errors. The imaginary part of the dispersion is 1 for all k, reflecting that all emitters search the atomic limit with the decay rate equal to the spontaneous emission without a light line, i.e., collective emission is absent.

B. Alternating quantum emitters

Having introduced the properties of long-range hopping subwavelength atomic arrays, we consider a two-band model—a 1D array of two different alternating arranged species of quantum emitters with transition energies $\omega_0 \pm h$ in free space, as illustrated in Fig. 1 [31]. We expect the Born-Markov approximation $\mathbf{G}(\mathbf{r}_i, \mathbf{r}_j, \omega) \simeq \mathbf{G}(\mathbf{r}_i, \mathbf{r}_j, \omega_0)$ remains to behold, as the relative difference between $\mathbf{G}(\mathbf{r}_i, \mathbf{r}_j, \omega_0 \pm h)$ and $\mathbf{G}(\mathbf{r}_i, \mathbf{r}_j, \omega_0)$ is of order h/ω_0, which is negligible provided that $h \ll \omega_0$ [32]. Note that similar approximations are used in, e.g., Ref. [33], where a magnetic field is applied to induce a Zeeman splitting. The corresponding Hamiltonian

$$H_{\mathrm{TB}} = H_{\mathrm{RDDI}} + h\sum_{j=1}^{N}(-1)^{j+1}\sigma_j^\dagger\sigma_j \tag{6}$$

is block-diagonalizable in the quasimomentum space in the infinite-array limit. To see this, we write the long-range hopping terms explicitly,

$$H_{\mathrm{TB}} = -\sum_{i=-\infty}^{\infty}\sum_{n\in\mathbb{Z}\setminus\{0\}} G(nd)\sigma_{i+n}^\dagger\sigma_i + h\sum_{j=-\infty}^{\infty}(-1)^{j+1}\sigma_j^\dagger\sigma_j,$$

and introduce the Fourier transformed spin operators $o_k^\dagger = \sqrt{2/N}\sum_{j=1}^{N/2} e^{ikr_{2j-1}}\sigma_{2j-1}^\dagger$, $e_k^\dagger = \sqrt{2/N}\sum_{j=1}^{N/2} e^{ikr_{2j}}\sigma_{2j}^\dagger$, and $dk \in (-\pi/2, \pi/2]$ for the odd and even sites. The $n = 0$ term is added in all calculations using the procedure above Eq. (5). Rewriting Eq. (6) in the quasimomentum space leads to

$$H_{\mathrm{TB}} = \sum_k \begin{pmatrix} o_k^\dagger & e_k^\dagger \end{pmatrix} \tilde{H}_{\mathrm{TB}}(k) \begin{pmatrix} o_k \\ e_k \end{pmatrix}, \tag{7}$$

where

$$\tilde{H}_{\mathrm{TB}}(k) = \begin{pmatrix} h - \sum_{n\in\mathbb{Z}\setminus\{0\}} e^{-ik2dn} G(2dn) & -e^{-ikd}\sum_{n=-\infty}^{\infty} e^{-i(2n-1)kd} G[(2n-1)d] \\ -e^{ikd}\sum_{n=-\infty}^{\infty} e^{-i(2n-1)kd} G[(2n-1)d] & -h - \sum_{n\in\mathbb{Z}\setminus\{0\}} e^{-ik2dn} G(2dn) \end{pmatrix}.$$

Noting that the sum in the off-diagonal component is

$$\sum_{n=-\infty}^{\infty} e^{-i(2n-1)kd} G[(2n-1)d] = \sum_{n\in\mathbb{Z}\setminus\{0\}} \left[e^{-ikdn} G(dn) - e^{-ik2dn} G(2dn)\right] = \tilde{G}_d(k) - \tilde{G}_{2d}(k),$$

we obtain the following simple form for the two-band Bloch Hamiltonian:

$$\tilde{H}_{\mathrm{TB}}(k) = \begin{pmatrix} h - \tilde{G}_{2d}(k) & -e^{-ikd}[\tilde{G}_d(k) - \tilde{G}_{2d}(k)] \\ -e^{ikd}[\tilde{G}_d(k) - \tilde{G}_{2d}(k)] & -h - \tilde{G}_{2d}(k) \end{pmatrix}. \tag{8}$$

III. EXCEPTIONAL-POINT PHASE TRANSITION

The spatially alternating transition energies divides N atoms into two sublattices and leads to the formation of two bands with a dispersion relation

$$\omega_{\mathrm{eff}}^{\pm}(k) = -\tilde{G}_{2d}(k) \pm \sqrt{\left[\tilde{G}_d(k) - \tilde{G}_{2d}(k)\right]^2 + h^2} \tag{9}$$

in the infinite-array limit. Here, the two eigenvectors coalesce at fine-tuned parameters known as the exceptional points, where the Hamiltonian becomes nondiagonalizable. A necessary condition for the emergence of EPs is

$$-h^2 = [\tilde{G}_d(k) - \tilde{G}_{2d}(k)]^2, \tag{10}$$

which relates the differences in transition energies to the dispersions in the identical array limit $h = 0$. Recall that the collective decay rate is a constant in the long-range hopping limit (cf. Fig. 2) and the light line coincides with the new first Brillouin zone edge $k = \pi/(2d)$. The real parts of the dispersion $\tilde{G}(k)$ in the identical array limit at both interatomic distances d and $2d$ experience a cusp at $k = \pi/(2d)$ and match exactly for other k. Therefore, the two-band Hamiltonian satisfies the necessary condition Eq. (10) for nondiagonalizability for every $k \neq \pi/(2d)$ at $h_{\mathrm{EP}} = 0.5$. This is because the imaginary parts of $\tilde{G}_d(k) - \tilde{G}_{2d}(k)$ have an absolute value $1/2$ for $|k| \neq \pi/(2d)$, which can be readf from Fig. 2(b). Moreover, one can indeed confirm the nondiagonalizability from the Jordan form of Eq. (8) at $h = h_{\mathrm{EP}}$:

$$\tilde{H}_{\mathrm{TB}}(k) = V(k)\begin{pmatrix} -\tilde{G}_{2d}(k) & 1 \\ 0 & -\tilde{G}_{2d}(k) \end{pmatrix} V(k)^{-1},$$

$$V(k) = \begin{pmatrix} e^{-ikd} & 0 \\ i & \frac{1}{ih_{\mathrm{EP}}} \end{pmatrix}, \tag{11}$$

where $|k| < \pi/(2d)$. Due to this peculiar feature that the *whole* system (except the band edges) undergoes an EP transition, we call the phenomenon *EP phase transition*. In total, there are $N/2 - 1$ many two-level EPs at this point. Physically speaking, as h increases, the spontaneous emission mechanism changes from collective to individual in a square-root fashion [see Fig. 3(d)]. Here, the choice of an interatomic distance to be $k_0 d = \pi/2$ is crucial for maximizing the number of EPs at a fixed h. For small deviations from this special interatomic distance, $\tilde{H}_{\mathrm{TB}}(k)$ is diagonalizable in general for $h = h_{\mathrm{EP}}$; instead, the EP phase transition becomes a shape crossover from collective to atomic decay, see Appendix A.

The EP phase transition (collective-atomic emission transition) is analogous to the metal-insulator transition in the Aubry-André-Harper (AAH) model [34,35], where the localization transition occurs *simultaneously* at the full energy spectrum. In the usual short-range $\mathcal{PT}$-symmetric 1D models [36,37], the EP is analogous to the mobility edge in a generalized AAH model [38–40], and the (de)localized regions correspond to $\mathcal{PT}$-broken(symmetric) regions.

Figure 3 shows the finite chain spectrum for $N = 100$ to confirm the infinite chain prediction; there are $N/2 - 1$ EPs near $h = h_{\mathrm{EP}} = 0.5$. Furthermore, it is useful to consider the smallest angle between all pairs of normalized right eigenvectors

$$\alpha_m = \min_{i\neq j} \arccos\left(\left|\langle\psi_i^R|\psi_j^R\rangle\right|\right), \tag{12}$$

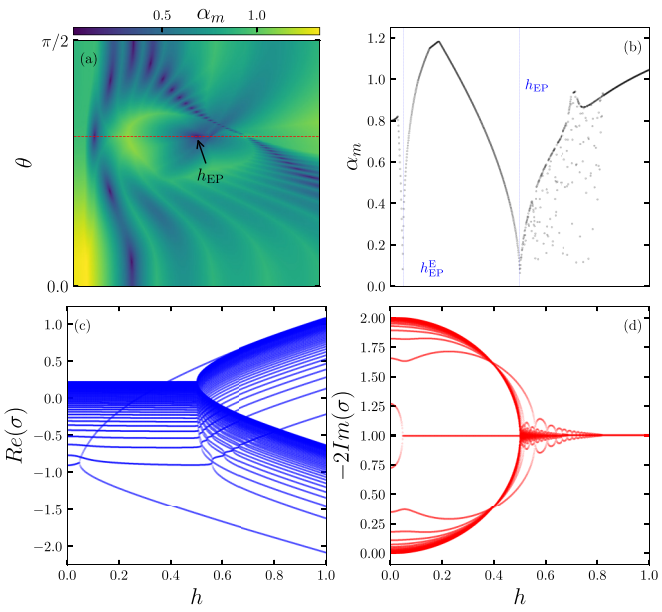

FIG. 3. Finite chain OBC calculation of (a) the smallest angle between all pairs of right eigenvectors for $N = 40$, $k_0 d = \pi/2$, and all possible θ, h. The red dotted line indicates the long-range hopping θ considered in the main text. EPs are commonly found in the parameter space [41]. (b) The smallest angle between all pairs of right eigenvectors (12) for $N = 100$. It signals the predicted EP phase transition at $h = 0.5$ and finite size induced $h_{\mathrm{EP}}^{\mathrm{E}}$ of the edge state Jordan block. (c and d) The real and imaginary parts of the spectrum σ for $N = 100$. The imaginary part is multiplied by -2 to make the atomic emission rate equal to 1. For $h < 0.5$, the spectrum is imaginary line gapped. In the infinite-array limit, the system contains $N/2 - 1$ two-level EPs at the EP transition point $h = 0.5$. The finite chain exact diagonalization spectrum gives a good agreement for states away from the light line.

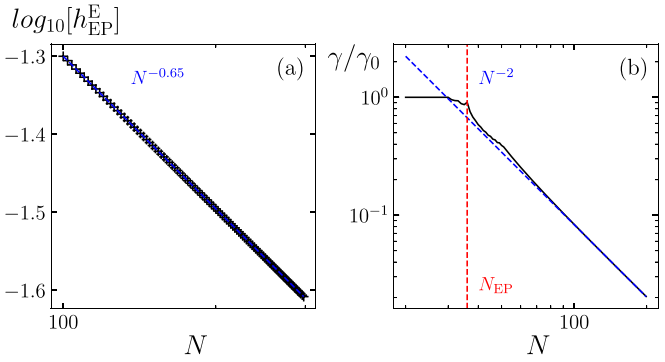

FIG. 4. Exact diagonalization results for (a) the finite size scaling of $h^{\mathrm{E}}_{\mathrm{EP}}$. The system shows a localized edge state for arbitrary small h greater than $N^{-0.65}$. (b) The subradiance scaling for $h = 20/N$. The ED result is shown in black and the blue dashed line shows the predicted N^{-2} scaling for large N. The ED result is captured by the infinite chain dispersion given in Eq. (9). This implies that small imperfection in transition energies would change the RDDI N^{-3} subradiance scaling.

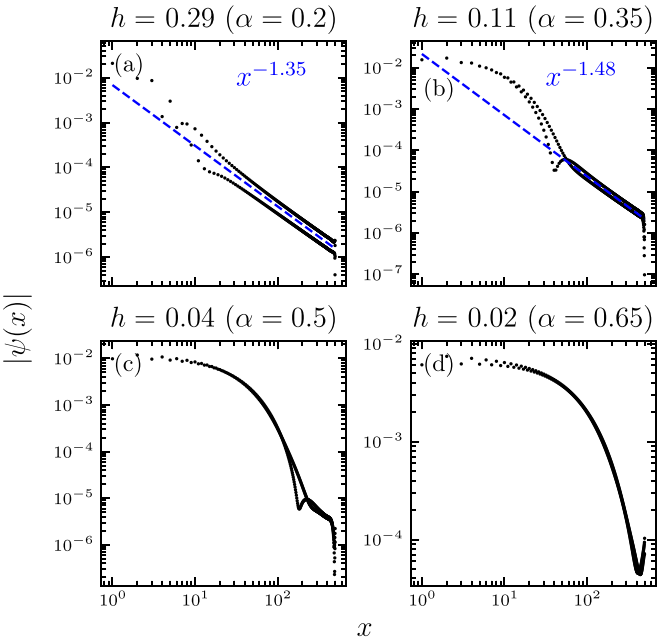

FIG. 5. Real-space distribution $|\psi(x)|$ of edge state at four different $h = N^{-\alpha}$ for $N = 500$. For $h < h^{\mathrm{E}}_{\mathrm{EP}} < h_{\mathrm{EP}} = 0.5$, the localization length of the edge state is extensive in system size. Once h overcomes the finite size threshold $h^{\mathrm{E}}_{\mathrm{EP}}$, the edge state becomes localized and shows a clear power-law decaying tail owing to the long-range nature of the model.

which goes to zero toward EPs and remains $\pi/2$ for diagonalizable spectrum degeneracies [42].

The angle metric also detects an EP at $h^{\mathrm{E}}_{\mathrm{EP}} \approx 0.05$ due to the finite size effect. This 2×2 block has the lowest real eigenvalues that match the $k = \pi/(2d)$ states in Fig. 2, and the corresponding eigenvectors are the span. Note that the infinite-array limit of $\tilde{H}_{\mathrm{TB}}[k = \pi/(2d)]$ is always diagonal, because $\tilde{G}_d(k)$ is discontinuous and coincides with $\tilde{G}_{2d}(k)$ at the light line. The open chain correction consists of a Fourier sum error of $\sin(r)/r$ that is bounded by $1/N$ known as the Gibbs phenomenon [43], and systematic finite size error when approximating the true finite array eigenstates by the Bloch states. The finite-size *Ansatz* error scaling of subradiance is discussed in Refs. [10,11,44], but such behavior is absent for states in the middle of the decay spectrum, which stops us from gaining an analytic finite size scaling. We numerically find that $h^{\mathrm{E}}_{\mathrm{EP}}$ goes to zero in the infinite chain limit with a $N^{-0.65}$ power-law scaling as shown in Fig. 4(a).

In addition, we find the position of EP around $h \approx 0.55$ remains for larger N, which is not captured by Eq. (10). The quasimomenta of this pair of states are identified by tracking their eigenvalues in the $h = 0$ limit; they are the states that have the closest k from the light line. Unlike the localized light line state, the pair of states here are delocalized in the real space. Due to the singular behavior of Green's tensor, the above infinite chain results are expected to hold only for states with quasimomentum away from the light line.

Recently, the power law exponent α for the subradiant states was unraveled being the power-law scaling behavior of group velocity $\partial\omega_{\mathrm{eff}}/\partial k$ near the band edge $k = \pi/d$, more precisely $\alpha = s + 1$ and $\omega_k - \omega_{\pi/d} \propto (k - \pi/d)^s$ [44], and closely related to the overlap error between a set of finite chain *Ansätze* and the Bloch states [10]. However, such scaling and *Ansätze* break down near the light line $k = \pm k_0$ [11,44]. Having two species of quantum emitters arranged alternatively at the discussed parameters, the macroscopic number of EPs can influence the subradiance scaling. The new dispersion relation Eq. (9) implies a change in subradiance scaling for small differences in transition energies. For $h = 0$, such scaling of Eq. (1) is N^{-3} due to the quadratic dispersion at the band edge, as the smallest nonvanishing expansion order in k of $\Re[\tilde{G}_d(k)]$ near $k = \pi/d$ is 2 [44]. Similarly, the dispersion of the two-band model is given by Eq. (9), and expansion in small h yields a new overall subradiance scaling, $O(N^{-3}) + O(h^2)$. Thus, we take $h = N^{-\alpha}$ to observe a valid scaling, and collective emission is suppressed for any $h > h_{\mathrm{EP}} = 0.5$. Evidently, the RDDI scaling is recovered if $\alpha \geqslant 3/2$. Otherwise, the scaling is dominated by h if $\alpha < 3/2$. Figure 4 shows the scaling transition for $h = 20/N$. The most subradiant decay rate is in the same order as the spontaneous emission rate γ_0 for $N < N_{\mathrm{EP}} = 40$, i.e., $h \geqslant 0.5$ when $N \leqslant 40$. Further system size increases show the predicted N^{-2} scaling. Note that previous studies found that small disorder in atomic arrays suppresses the usual RDDI subradiant (N^{-3}) scaling [45]. Here, in contrast, we find a small alternative on-site potential makes the system more radiative.

IV. EDGE STATE

Having discussed the coalescence of the two $k = \pi/(2d)$ states from both bands at $h^{\mathrm{E}}_{\mathrm{EP}}$, we consider their real-space localization properties, as shown in Fig. 5 for a range of $h = N^{-\alpha}$. In a finite chain of $N = 500$ emitters, the spatial distribution $|\psi(x)|$ is localized at one end, and this localized state has an imaginary part of eigenvalue equal to the atomic spontaneous emission rate.

We identify this mode as a dissipation-induced edge state, in the sense that such localization is not observed when

discarding the dissipative part of the Hamiltonian. For $h < h_{\mathrm{EP}}^{\mathrm{E}}$ (Fig. 5 lower), we find the localization length of this wave function to be extensive in system size, such that its amplitude decreases to zero roughly at the opposite end of the chain. For $h > h_{\mathrm{EP}}^{\mathrm{E}}$, the real-space amplitude is truly localized and shows an algebraic decay tail, which has been numerically observed in other long-range models [46,47].

It is tempting to attribute the edge state to the nontrivial bulk properties of the model. Indeed, the number of edge states of a Hermitian short-range Hamiltonian is related to its bulk topological number, known as the bulk-edge correspondence, which has been generalized to non-Hermitian systems [12,15,48–50]. For example, the notion of band gap in real energy for Hermitian systems cannot capture the complex spectrum for non-Hermitian cases. One can generalize the notion of gap to lines that separate spectrum clusters in the complex plane, known as line gapped [18].

However, the topological properties of $\tilde{H}_{\mathrm{TB}}(k)$ is ill-defined due to the discontinuity of $\tilde{G}_d(k)$ in k [26]. In the following, we explain the ill-definedness in further detail and show that the edge state is *not* topologically protected, as it can be removed via a symmetry-preserving continuous deformation.

We consider the two-band model in the Su–Schrieffer–Heeger-like (SSH-like) form by rewriting Eq. (8) in terms of the spin-$\frac{1}{2}$ Pauli matrices $\sigma_{0,x,y,z}$ with $\tilde{G}_d(k) - \tilde{G}_{2d}(k) = ig(k)$, where

$$g(k) = \begin{cases} h_{\mathrm{EP}} & |k| < \frac{\pi}{2d} \\ 0 & k = \pm\frac{\pi}{2d} \\ -h_{\mathrm{EP}} & |k| > \frac{\pi}{2d} \end{cases}$$

is real. Note that $g(k)$ is a *discontinuous* function and changes its sign upon crossing the light line. This sign change ensures the periodicity $\tilde{H}_{\mathrm{TB}}(k + \pi/d) = \tilde{H}_{\mathrm{TB}}(k)$. Within $kd \in (-\pi/2, \pi/2]$, $\tilde{H}_{\mathrm{TB}}(k)$ reads

$$\begin{aligned}\tilde{H}_{\mathrm{TB}}(k) = &-\tilde{G}_{2d}(k)\sigma_0 + h\sigma_z - ig(k)\cos(kd)\sigma_x \\ &- ig(k)\sin(kd)\sigma_y. \end{aligned} \tag{13}$$

Strictly speaking, the spectrum is *separable* for a nonvanishing h, i.e., the two bands have no energy crossing for all quasimomentum [51]. Without the discontinuity, the spectrum is imaginary line gapped at $\Im\omega = \Im\tilde{G}_d[k = \pi/(2d)]$ for $h < h_{\mathrm{EP}}$, and separable for $h > h_{\mathrm{EP}}$.

Without loss of generality, the σ_0 term can be dropped since $\tilde{H}_{\mathrm{TB}}(k)$ can be continuously connected to a Hamiltonian $\tilde{H}'_{\mathrm{TB}}(k)$ without σ_0 [52]:

$$\tilde{H}'_{\mathrm{TB}}(k) = h\sigma_z - ig(k)\cos(kd)\sigma_x - ig(k)\sin(kd)\sigma_y. \tag{14}$$

This model appears to be similar to a short-range $\mathcal{PT}$-symmetric SSH model [36]. Despite the similarity, the latter has a pair of edge states at two ends of the chain, and they are topologically protected. As shown in Appendix B, Hermitization of the short-range SSH model leads to a well-defined winding number $\mathbb{Z}$. In the former case, the range of quasimomentum is only defined as half of the Brillouin zone of the latter, over which we can simplify Eq. (14) into

$$\tilde{H}'_{\mathrm{TB}} = h\sigma_z - ih_{\mathrm{EP}}\cos(kd)\sigma_x - ih_{\mathrm{EP}}\sin(kd)\sigma_y. \tag{15}$$

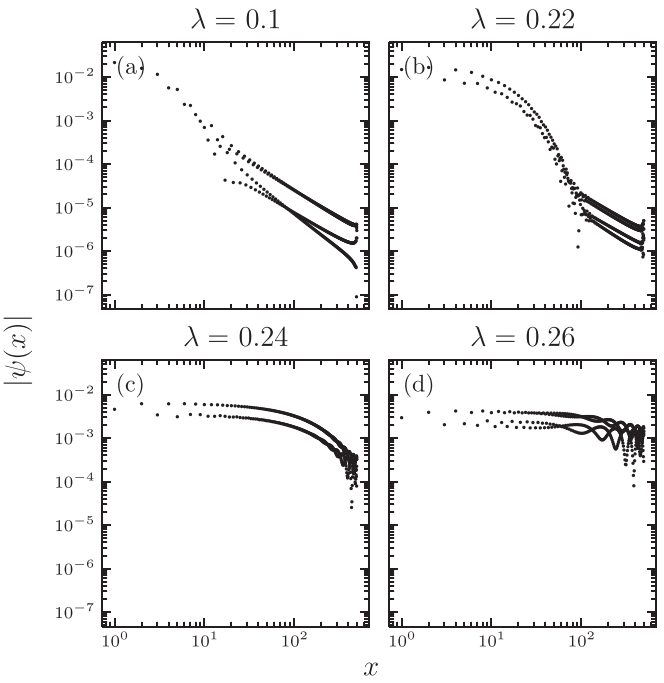

FIG. 6. Edge state of the deformed Hamiltonian (16). The real-space amplitude $|\psi(x)|$ is shown at four different λ for $N = 500$ and $h = N^{-0.25} \approx 0.21$. Increasing λ delocalizes the power-law tailed edge state, which indicates that it is not symmetry protected.

While the above expression appears to be continuous, it is discontinuous at $k = \pi/(2d)$ since the Brillouin zone is $dk \in (-\pi/2, \pi/2]$. Under the open boundary condition, we numerically find that only one of the states connected to $k = \pi/(2d)$ Bloch waves under the periodic boundary condition is an edge state while another is delocalized.

Since the edge state does not correspond to a well-defined bulk property, we consider a continuous deformation of Eq. (14) to a topologically trivial Hamiltonian

$$H(\lambda) = (1 - \lambda)\tilde{H}'_{\mathrm{TB}}(k) + \lambda H'' \quad \lambda \in [0, 1], \tag{16}$$

where $H'' = i\sigma_x$ such that both the pseudo-Hermiticity and imaginary line gap are preserved along the path. Figure 6 shows the real-space amplitude of the edge state at four different λ, where increasing λ gradually delocalizes the edge state.

V. QUANTUM WALKS

In the last section, we consider the real-time evolution of an initial state $|\psi_0\rangle$ under H_{TB}, known as the continuous-time quantum walk [53]. Under such nonunitary time evolution, the spontaneous emission occurs during $[t, t + dt]$ with a probability $-2\langle\psi(t)|\Im(H_{\mathrm{TB}})|\psi(t)\rangle dt$, where $|\psi(t)\rangle = e^{-iH_{\mathrm{TB}}t}|\psi_0\rangle$. We are interested in how the spontaneous emission can be resolved spatially.

Owning the experimental developments of spatially local quantum controls [54], previous works have mostly focused on non-Hermitian Hamiltonians with on-site loss [55]. The anti-Hermitian part of such a Hamiltonian is diagonal in the real space. Hence, the emission (escape) probability from a site x is proportional to $\int_0^\infty |\langle x|\psi(t)\rangle|^2 dt$, where $|x\rangle = \sigma_x^\dagger|\mathbf{g}\rangle$. On the other hand, photon-mediated interactions consist of

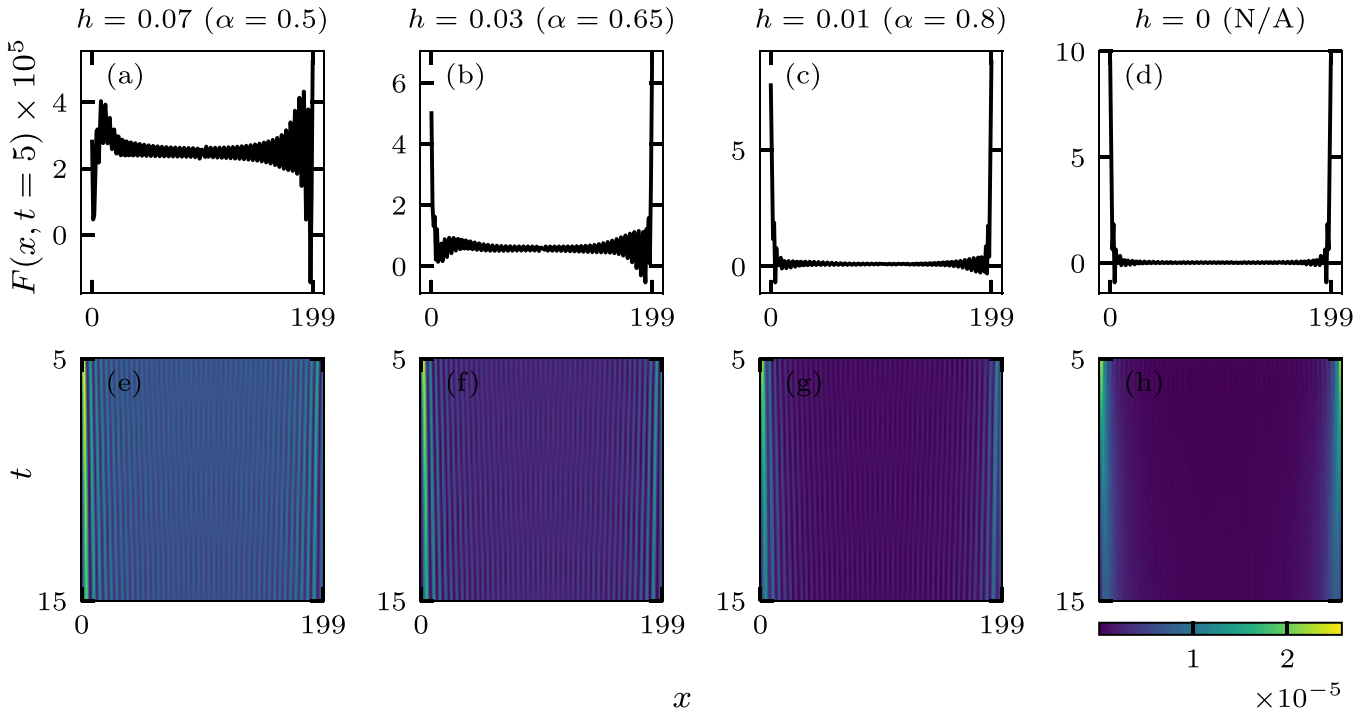

FIG. 7. Quantum walk results at four different $h = N^{-\alpha}$ for $N = 200$. The RDDI is recovered for $h = 0$. The initial state $(\sum_{i=1}^{N} \sigma_i^\dagger |\mathbf{g}\rangle)/\sqrt{N}$ is parity symmetric. (Upper) Due to the fast escape rate of radiant states, the short-time limit is excluded. The late-time ($t = 5$) escape distribution Eq. (17) shows an asymmetric escape tendency. The emission occurs predominantly at the boundaries of the chain without the edge state. Only top left figure $h = 0.07$ supports the edge state, showing that the existence of the edge state dramatically enhances emission from the bulk. (Lower) A late-time interval wave-function density, $|\langle x|\psi(t)\rangle|^2$ shows a similar imbalance, where the wave function has the greatest overlap with the edge state.

long-range dissipative hopping, as is the case here, $\Im H_{\mathrm{TB}} = i(H_{\mathrm{TB}}^\dagger - H_{\mathrm{TB}})/2$ is no longer diagonal. Therefore, we consider a generalized spatially resolved escape distribution

$$F(x,t) = -\int_t^\infty dt' \langle\psi(t')|\{|x\rangle\langle x|, \mathrm{Im}H_{\mathrm{TB}}\}|\psi(t')\rangle, \quad (17)$$

where $\{A, B\} = AB + BA$ and clearly reproduces the conventional definition for on-site loss. The normalization property $\sum_x F(x, 0) = 1$ is shown in Appendix C.

In general, $F(x, 0)$ is real but not necessarily positive, so it is a quasi-probability distribution, just like the Wigner function [56]. The physical intuition behind the negative escape quasi-probability will be explained in the following.

This generalization is motivated from the following decomposition of $d|\langle x|\psi(t)\rangle|^2/dt$:

$$\frac{d}{dt}|\langle x|\psi(t)\rangle|^2 = -i\langle\psi(t)|[|x\rangle\langle x|, \mathrm{Re}H_{\mathrm{TB}}]|\psi(t)\rangle + \langle\psi(t)|\{|x\rangle\langle x|, \mathrm{Im}H_{\mathrm{TB}}\}|\psi(t)\rangle. \quad (18)$$

The first term on the right-hand side may be interpreted as a coherent current, which persists in the Hermitian limit. The second term is unique to non-Hermitian systems and may be interpreted as incoherent current, including both on-site loss and dissipative hopping from/to other sites. Therefore, due to the non-Hermiticity of the long-range hopping terms, there are incoherent flows between different sites that can lead to net gain at certain sites.

Returning to the time domain, we know that the short- and late-time dynamics generated by H_{TB} are dominated by radiant and subradiant states. The presence of radiant states promotes a rapid exponential fast escape rate in the short-time limit and dilutes the intensity of late-time emission [31]. Despite this experimental challenge, we are ideally interested in the spatially resolved late-time dynamics from $t = 5$.

Figure 7 (upper) shows the late-time escape distribution $F(x, t = 5)$ by propagating the initial state $|\psi_0\rangle = (\sum_{i=1}^{N} \sigma_i^\dagger |\mathbf{g}\rangle)/\sqrt{N}$, the so-called W state [57]. The lower panel shows the space-time resolved wave-function density $|\langle x|\psi(t)\rangle|^2$ from the same initial state under such nonunitary dynamics as a complementary observable.

For the RDDI model H_{RDDI} (i.e., H_{TB} with $h = 0$), the excitation is mostly likely to escape from both edges of the atomic chain, which is consistent with the numerical finding of the electric field intensity of the subradiant eigenstates in Ref. [10].

For a small h, the winding number of H_{TB} is not well defined due to the long-range nature of this model. Hence, novel non-Hermitian dynamical phenomena related to bulk topological properties, such as the quantization of walker displacement [58] and edge burst under on-site losses [55], are not observed. However, the existence of an edge state influences the late-time dynamics. For $h < h_{\mathrm{EP}}^{\mathrm{E}}$, none of the eigenstates are localized, and the excitation is most likely to escape from the boundaries. For $h > h_{\mathrm{EP}}^{\mathrm{E}}$, we find the disappearance of the boundary concentration and the rise of bulk emission.

In addition, the escape distribution is asymmetric under parity, while the initial state is symmetric. This is reasonable since the alternating potential explicitly breaks the parity symmetry. This effect is more visible in the time evolution of density—Fig. 7 (lower panels) shows an imbalance across the chain and density accumulation toward the edge state, which reflects that the late-time wave function is mostly supported on the edge state.

VI. CONCLUSION

We have studied the long-range hopping limit of the RDDI Hamiltonian, where the hopping power equals the lattice dimension—a realistic model for an atomic array in 3D free space. Arranging two species of quantum emitters alternatively, we find the new dispersion relation has a simple form in the infinite chain limit and encodes a novel non-Hermitian behavior, dubbed exceptional-point phase transition. At the transition point, each pair of eigenvectors coalesce, except for the two states from each band with the quasi-momentum $k = \pi/(2d)$.

For a finite chain, the differences in transition energies modify the N^{-3} subradiance scaling law and accelerate the most subradiant decay rate. The spectrum of finite calculation shows a good agreement with EP phase transition.

We numerically show that one of the $k = \pi/(2d)$ states is adiabatically connected to a boundary localized state in real space under the open boundary condition, while another remains delocalized. The localized state has a power-law tail for any h greater than the finite size threshold scaling as $N^{-0.65}$. The presence of the light line generates discontinuities in the dispersion, which makes the winding number ill-defined.

Finally, we have generalized the spatial escape distribution for on-site dissipative models to nonlocal dissipation. For a quantum walker starting from a parity symmetric initial state, both the late-time escape distribution and wave-function density show spatial imbalances.

Our work has only focused on 1D arrays in 3D free space. It is natural to consider higher-dimensional arrays [33], as well as more general (artificial) photonic environments such as waveguides and photonic crystals that may be engineered to be intrinsically topological or/and dissipative [22]. It would be interesting to construct more models that exhibit the EP phase transition, to study the topological properties and bulk-edge correspondence, and to explore the rich dynamics of incoherent and collective atomic decay.

ACKNOWLEDGMENTS

J.L. thanks R. Schäfer, D. J. Luitz, F. Piazza, Z. Wang, and L. Piroli for interesting discussions, also Y. E. Zhang for providing technical support for the illustration figure. Z.G. thanks D. Wild for lecturing on the basics of subwavelength atomic arrays. J.L. acknowledges support from Deutsche Forschungsgemeinschaft through the project DQUANT (Project No. 499347025) and the Erwin Schrödinger International Institute for Mathematics and Physics for its hospitality during the Thematic programme Tensor Networks: Mathematical Structures and Novel Algorithms. Z.G. was supported by The University of Tokyo Excellent Young Researcher Program.

APPENDIX A: OTHER CHOICES OF INTERATOMIC DISTANCES

For the fine-tuned interatomic distances $k_0 d = \pi/2$, the alternating array defined by Eq. (8) is shown to have an EP phase transition at h_{EP} both analytically and numerically; the Hamiltonian is typically diagonalizable and a macroscopic number of EPs requires parameter fine tuning. Here, we consider the effect of small deviations in the interatomic distances. Figure 8 shows the eigenvalues of Eq. (8) at two other interatomic distances, $k_0 d = 0.495\pi$ and $k_0 d = 0.49\pi$. The spectrum displays a similar shape to Fig. 3, but the system has a finite gap at h_{EP} and no longer shows a genuine EP transition. Instead, there is a sharp crossover from collective to atomic decay.

APPENDIX B: TOPOLOGICAL INVARIANT FOR SHORT-RANGE CHIRAL-SYMMETRIC SYSTEMS

In the main text, we have established that the long-range hopping two-band model $\tilde{H}'_{\mathrm{TB}}(k)$ has the SSH-like form (14), with a quasimomentum $kd \in (-\pi/2, \pi/2]$ and a discontinuous off-diagonal matrix element $g(k)$. Here, we consider the topological invariant of its short-range analogy H_{SR}, where the quasimomentum is defined as $kd \in (-\pi, \pi]$ and the off-diagonal element $g(k) = g$ is a real constant.

Point-gapped non-Hermitian systems encounter novel features without Hermitian counterparts, such as the skin effect [17,59,60]. However, a line-gapped system can always be mapped onto a Hermitian system, as is the case

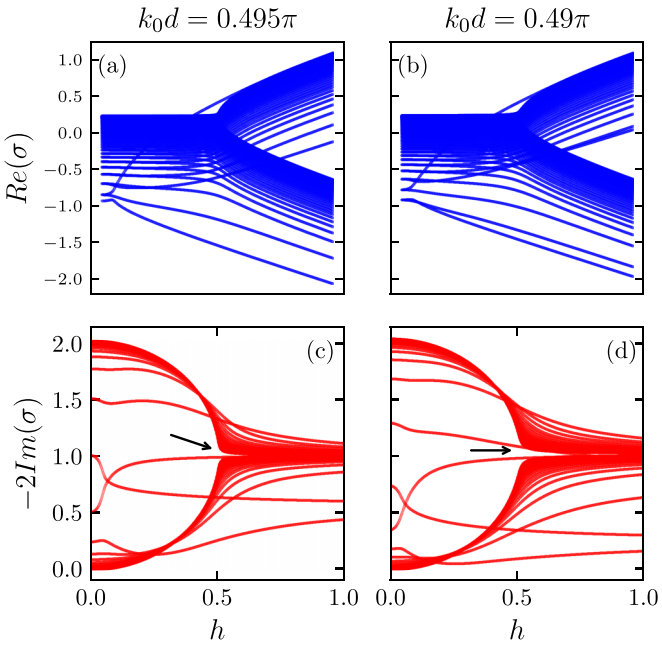

FIG. 8. The real (a) and (b) and imaginary (c) and (d) parts of the spectrum σ for $k_0 d = 0.495$, $k_0 d = 0.49\pi$, and $N = 100$. The inserted black arrow in (c) and (d) indicates a finite gap at h_{EP}, which means the EP transition is not observed.

here [12,18,61]. To perform the Hermitization of the two-band model, we first note that $i\sigma_x, i\sigma_y$, and σ_z forms a $SU(1,1)$ algebra [62]. Consequently, $H_{\mathrm{TB}}(k)$ exhibits the pseudo-Hermiticity:

$$\eta H_{\mathrm{SR}}(k)\eta = H_{\mathrm{SR}}(k)^\dagger, \quad \eta = \sigma_z.$$

We multiply $H_{\mathrm{SR}}(k)$ by i [63],

$$iH_{\mathrm{SR}}(k) = ih\sigma_z + g\cos(kd)\sigma_x + g\sin(kd)\sigma_y, \tag{B1}$$

to turn the imaginary line gap into a real gap. The pseudo-Hermiticity transforms into pseudo-anti-Hermiticity, which may also be called chiral symmetry [18]:

$$\eta H_{\mathrm{SR}}(k)\eta = -H_{\mathrm{SR}}(k)^\dagger \quad \eta = \sigma_z.$$

The winding number of $iH_{\mathrm{SR}}(k)$ can be defined by using the following projection operators:

$$P_1(k) = |R_+(k)\rangle\langle L_+(k)|, \quad P_2(k) = |L_-(k)\rangle\langle R_-(k)|,$$

where $|R_\pm(k)\rangle$ ($|L_\pm(k)\rangle$) are the right (left) eigenvectors of $H_{\mathrm{SR}}(k)$, to construct a Hermitian operator

$$\begin{aligned} Q(k) &= 1 - (P_1(k) + P_2(k)) = \frac{1}{\sqrt{g^2 - h^2}}\begin{pmatrix} 0 & ge^{-ikd} \\ ge^{ikd} & 0 \end{pmatrix} \\ &= \begin{pmatrix} 0 & q(k) \\ q^*(k) & 0 \end{pmatrix}, \end{aligned} \tag{B2}$$

which is Hermitian and chiral symmetric:

$$\Gamma Q(k)\Gamma = -Q(k), \quad \Gamma = \sigma_z.$$

Technically speaking, $Q(k)$ belongs to class BDI of the Altland-Zirnbauer classification [64] and is characterized by the winding number $\int_{\mathrm{B.Z.}} \frac{dk}{2\pi i} q(k)^{-1}\partial_k q(k) \in \mathbb{Z}$ for a continuous $q(k)$. Therefore, the topological invariant for the short-range non-Hermitian SSH model can be defined.

In the case of our long-range Hamiltonian $H'_{\mathrm{TB}}(k)$, we can identify the corresponding $q(k)$ following a similar procedure. However, the discontinuity of $q(k)$ at $k = \pi/(2d)$ prohibits us from concluding a quantized winding number.

APPENDIX C: NORMALIZATION PROPERTY OF $F(x,t)$

We show the generalized spatially resolved escape distribution $F(x,t)$ is normalized for $t = 0$. For a normalized initial state $\langle\psi_0|\psi_0\rangle = 1$ and H_{TB} with a complex spectrum $\{E_n\}$ that lies only on the lower half of the complex energy plane, summing over space gives

$$\begin{aligned} \sum_x F(x,0) &= -\sum_x \int_0^\infty dt' \langle\psi(t')|\{|x\rangle\langle x|, \mathrm{Im}H_{\mathrm{TB}}\}|\psi(t')\rangle \\ &= -2\int_0^\infty dt' \langle\psi(t')|\mathrm{Im}H_{\mathrm{TB}}|\psi(t')\rangle \\ &= -\int_0^\infty dt' \, \langle\psi(t')|\, iH_{\mathrm{TB}}^\dagger - iH_{\mathrm{TB}}\,|\psi(t')\rangle \\ &= -\int_0^\infty dt' \frac{d}{dt'}\,\langle\psi(t')|\,|\psi(t')\rangle \\ &= \langle\psi_0|\psi_0\rangle - \langle\psi_\infty|\psi_\infty\rangle = 1, \end{aligned}$$

where $|\psi_\infty\rangle = \lim_{t\to\infty} e^{-iH_{\mathrm{TB}}t}\,|\psi_0\rangle = 0$ regardless of the diagonalizability of H_{TB}. To see this, we consider following spectral decomposition of H_{TB} in the Jordan normal form [12]:

$$\begin{aligned} \|e^{-iH_{\mathrm{TB}}t}\| &= \left\| \sum_n e^{-iE_n t}\left(P_n + \sum_{i=1}^{m_n^g}\sum_{j=1}^{n_i-1} \frac{t^j}{j!} N_{n_i}^j \right) \right\| \\ &\leqslant \sum_n e^{\Im(E_n)t} \left\| \left(P_n + \sum_{i=1}^{m_n^g}\sum_{j=1}^{n_i-1} \frac{t^j}{j!} N_{n_i}^j \right) \right\|, \end{aligned}$$

where for each Jordan block with eigenvalue E_n, P_n is the set of orthogonal and complete projectors, m_n^g is the geometric multiplicities, and N_{n_i} is a nilpotent off-diagonal block with size n_i. Because $\{\Im(E)\}$ lies below the real axis, the exponential term decreases faster than the polynomial growth, and thus the above equation vanishes in the limit of $t \to \infty$. We mention that it is necessary to assume a finite system and take this infinite time limit first. Otherwise, if the sizes of some Jordan blocks grow with the system size, the polynomial contribution may dramatically enlarge the relaxation time, possibly to infinity in the thermodynamic limit. This occurs in some systems exhibiting the non-Hermitian skin effect [65].

[1] E. Shahmoon, D. S. Wild, M. D. Lukin, and S. F. Yelin, Cooperative resonances in light scattering from two-dimensional atomic arrays, Phys. Rev. Lett. **118**, 113601 (2017).

[2] D. E. Chang, J. S. Douglas, A. González-Tudela, C.-L. Hung, and H. J. Kimble, *Colloquium:* Quantum matter built from nanoscopic lattices of atoms and photons, Rev. Mod. Phys. **90**, 031002 (2018).

[3] M. Manzoni, M. Moreno-Cardoner, A. Asenjo-Garcia, J. V. Porto, A. V. Gorshkov, and D. Chang, Optimization of photon storage fidelity in ordered atomic arrays, New J. Phys. **20**, 083048 (2018).

[4] T. L. Patti, D. S. Wild, E. Shahmoon, M. D. Lukin, and S. F. Yelin, Controlling interactions between quantum emitters using atom arrays, Phys. Rev. Lett. **126**, 223602 (2021).

[5] M. Moreno-Cardoner, D. Goncalves, and D. E. Chang, Quantum nonlinear optics based on two-dimensional Rydberg atom arrays, Phys. Rev. Lett. **127**, 263602 (2021).

[6] K. Srakaew, P. Weckesser, S. Hollerith, D. Wei, D. Adler, I. Bloch, and J. Zeiher, A subwavelength atomic array switched by a single Rydberg atom, Nat. Phys. **19**, 714 (2023).

[7] W. Guerin, M. O. Araújo, and R. Kaiser, Subradiance in a large cloud of cold atoms, Phys. Rev. Lett. **116**, 083601 (2016).

[8] G. Ferioli, A. Glicenstein, L. Henriet, I. Ferrier-Barbut, and A. Browaeys, Storage and release of subradiant excitations in a dense atomic cloud, Phys. Rev. X **11**, 021031 (2021).

[9] A. S. Sheremet, M. I. Petrov, I. V. Iorsh, A. V. Poshakinskiy, and A. N. Poddubny, Waveguide quantum electrodynamics: Collective radiance and photon-photon correlations, Rev. Mod. Phys. **95**, 015002 (2023).

[10] A. Asenjo-Garcia, M. Moreno-Cardoner, A. Albrecht, H. J. Kimble, and D. E. Chang, Exponential improvement in photon storage fidelities using subradiance and "selective radiance" in atomic arrays, Phys. Rev. X **7**, 031024 (2017).

[11] Y.-X. Zhang and K. Mølmer, Theory of subradiant states of a one-dimensional two-level atom chain, Phys. Rev. Lett. **122**, 203605 (2019).

[12] Y. Ashida, Z. Gong, and M. Ueda, Non-Hermitian physics, Adv. Phys. **69**, 249 (2020).

[13] W. D. Heiss, The physics of exceptional points, J. Phys. A: Math. Theor. **45**, 444016 (2012).

[14] E. J. Bergholtz, J. C. Budich, and F. K. Kunst, Exceptional topology of non-Hermitian systems, Rev. Mod. Phys. **93**, 015005 (2021).

[15] S. Yao and Z. Wang, Edge states and topological invariants of non-Hermitian systems, Phys. Rev. Lett. **121**, 086803 (2018).

[16] N. Okuma and M. Sato, Non-Hermitian topological phenomena: A review, Annu. Rev. Condens. Matter Phys. **14**, 83 (2023).

[17] Z. Gong, Y. Ashida, K. Kawabata, K. Takasan, S. Higashikawa, and M. Ueda, Topological phases of non-Hermitian systems, Phys. Rev. X **8**, 031079 (2018).

[18] K. Kawabata, K. Shiozaki, M. Ueda, and M. Sato, Symmetry and topology in non-Hermitian physics, Phys. Rev. X **9**, 041015 (2019).

[19] H. Zhou and J. Y. Lee, Periodic table for topological bands with non-Hermitian symmetries, Phys. Rev. B **99**, 235112 (2019).

[20] Z. Gong, M. Bello, D. Malz, and F. K. Kunst, Anomalous behaviors of quantum emitters in non-Hermitian baths, Phys. Rev. Lett. **129**, 223601 (2022).

[21] Z. Gong, M. Bello, D. Malz, and F. K. Kunst, Bound states and photon emission in non-Hermitian nanophotonics, Phys. Rev. A **106**, 053517 (2022).

[22] F. Roccati, M. Bello, Z. Gong, M. Ueda, F. Ciccarello, A. Chenu, and A. Carollo, Hermitian and non-Hermitian topology from photon-mediated interactions, arXiv:2303.00762

[23] L. Xiao, T. Deng, K. Wang, G. Zhu, Z. Wang, W. Yi, and P. Xue, Observation of non-Hermitian bulk-boundary correspondence in quantum dynamics, Nat. Phys. **16**, 761 (2020).

[24] L. Xiao, W.-T. Xue, F. Song, Y.-M. Hu, W. Yi, Z. Wang, and P. Xue, Observation of non-Hermitian edge burst in quantum dynamics, arXiv:2303.12831.

[25] T. Kuwahara and K. Saito, Absence of fast scrambling in thermodynamically stable long-range interacting systems, Phys. Rev. Lett. **126**, 030604 (2021).

[26] Z. Gong, T. Guaita, and J. I. Cirac, Long-range free fermions: Lieb-Robinson bound, clustering properties, and topological phases, Phys. Rev. Lett. **130**, 070401 (2023).

[27] R. H. Lehmberg, Radiation from an n-atom system. I. General formalism, Phys. Rev. A **2**, 883 (1970).

[28] T. Gruner and D.-G. Welsch, Green-function approach to the radiation-field quantization for homogeneous and inhomogeneous Kramers-Kronig dielectrics, Phys. Rev. A **53**, 1818 (1996).

[29] S. Xu and S. Fan, Input-output formalism for few-photon transport: A systematic treatment beyond two photons, Phys. Rev. A **91**, 043845 (2015).

[30] T. Shi, D. E. Chang, and J. I. Cirac, Multi-photon scattering theory and generalized master equations, Phys. Rev. A **92**, 053834 (2015).

[31] M. Reitz, C. Sommer, and C. Genes, Cooperative quantum phenomena in light-matter platforms, PRX Quantum **3**, 010201 (2022).

[32] Rigorously speaking, this is true only when $r = |\mathbf{r}_i - \mathbf{r}_j|$ is not so large, as should be the case of experimentally accessible size of atomic arrays. Even if we consider the thermodynamic limit from a purely theoretical point of view, we realize that $G(r)$ itself is small for a sufficiently large r, so even a relative order one change is negligible.

[33] J. Perczel, J. Borregaard, D. E. Chang, H. Pichler, S. F. Yelin, P. Zoller, and M. D. Lukin, Topological quantum optics in two-dimensional atomic arrays, Phys. Rev. Lett. **119**, 023603 (2017).

[34] P. G. Harper, Single band motion of conduction electrons in a uniform magnetic field, Proc. Phys. Soc. London Sect. A **68**, 874 (1955).

[35] S. Aubry and G. André, Analyticity breaking and Anderson localization in incommensurate lattices, Ann. Isr. Phys. Soc. **3**, 18 (1980).

[36] A. F. Tzortzakakis, A. Katsaris, N. E. Palaiodimopoulos, P. A. Kalozoumis, G. Theocharis, F. K. Diakonos, and D. Petrosyan, Topological edge states of the $\mathcal{PT}$-symmetric Su-Schrieffer-Heeger model: An effective two-state description, Phys. Rev. A **106**, 023513 (2022).

[37] S. Weimann, M. Kremer, Y. Plotnik, Y. Lumer, S. Nolte, K. G. Makris, M. Segev, M. C. Rechtsman, and A. Szameit, Topologically protected bound states in photonic parity–time-symmetric crystals, Nat. Mater. **16**, 433 (2017).

[38] J. Biddle and S. Das Sarma, Predicted mobility edges in one-dimensional incommensurate optical lattices: An exactly solvable model of Anderson localization, Phys. Rev. Lett. **104**, 070601 (2010).

[39] S. Ganeshan, J. H. Pixley, and S. Das Sarma, Nearest neighbor tight binding models with an exact mobility edge in one dimension, Phys. Rev. Lett. **114**, 146601 (2015).

[40] Y. Wang, X. Xia, L. Zhang, H. Yao, S. Chen, J. You, Q. Zhou, and X.-J. Liu, One-dimensional quasiperiodic mosaic lattice with exact mobility edges, Phys. Rev. Lett. **125**, 196604 (2020).

[41] D. J. Luitz and F. Piazza, Exceptional points and the topology of quantum many-body spectra, Phys. Rev. Res. **1**, 033051 (2019).

[42] R. Schäfer, J. C. Budich, and D. J. Luitz, Symmetry protected exceptional points of interacting fermions, Phys. Rev. Res. **4**, 033181 (2022).

[43] K. F. Riley, M. P. Hobson, and S. J. Bence, *Mathematical Methods for Physics and Engineering: A Comprehensive Guide* (Cambridge University Press, Cambridge, 2006).

[44] Y.-X. Zhang and K. Mølmer, Subradiant emission from regular atomic arrays: Universal scaling of decay rates from the generalized Bloch theorem, Phys. Rev. Lett. **125**, 253601 (2020).

[45] D. F. Kornovan, N. V. Corzo, J. Laurat, and A. S. Sheremet, Extremely subradiant states in a periodic one-dimensional atomic array, Phys. Rev. A **100**, 063832 (2019).

[46] D. Vodola, L. Lepori, E. Ercolessi, and G. Pupillo, Long-range Ising and Kitaev models: Phases, correlations and edge modes, New J. Phys. **18**, 015001 (2015).

[47] S. B. Jäger, L. Dell'Anna, and G. Morigi, Edge states of the long-range Kitaev chain: An analytical study, Phys. Rev. B **102**, 035152 (2020).

[48] T. E. Lee, Anomalous edge state in a non-Hermitian lattice, Phys. Rev. Lett. **116**, 133903 (2016).

[49] F. K. Kunst, E. Edvardsson, J. C. Budich, and E. J. Bergholtz, Biorthogonal bulk-boundary correspondence in non-Hermitian systems, Phys. Rev. Lett. **121**, 026808 (2018).

[50] D. S. Borgnia, A. J. Kruchkov, and R.-J. Slager, Non-Hermitian boundary modes and topology, Phys. Rev. Lett. **124**, 056802 (2020).

[51] H. Shen, B. Zhen, and L. Fu, Topological band theory for non-Hermitian Hamiltonians, Phys. Rev. Lett. **120**, 146402 (2018).

[52] Rigorously speaking, the continuity is questionable as $\tilde{G}_{2d}(k)$ diverges at $k = \pm\pi/(2d)$. However, since the deformation is just a sublattice-independent energy shift, it is natural to expect no effect on band topology.

[53] A. M. Childs, On the relationship between continuous- and discrete-time quantum walk, Commun. Math. Phys. **294**, 581 (2010).

[54] S. Haroche and J.-M. Raimond, *Exploring the Quantum: Atoms, Cavities, and Photons* (Oxford University Press, New York, 2006).

[55] W.-T. Xue, Y.-M. Hu, F. Song, and Z. Wang, Non-Hermitian edge burst, Phys. Rev. Lett. **128**, 120401 (2022).

[56] C. Cohen-Tannoudji, J. Dupont-Roc, and G. Grynberg, *Atom-Photon Interactions: Basic Processes and Applications* (Wiley, New York, 1998).

[57] W. Dür, G. Vidal, and J. I. Cirac, Three qubits can be entangled in two inequivalent ways, Phys. Rev. A **62**, 062314 (2000).

[58] M. S. Rudner and L. S. Levitov, Topological transition in a non-Hermitian quantum walk, Phys. Rev. Lett. **102**, 065703 (2009).

[59] N. Okuma, K. Kawabata, K. Shiozaki, and M. Sato, Topological origin of non-Hermitian skin effects, Phys. Rev. Lett. **124**, 086801 (2020).

[60] K. Zhang, Z. Yang, and C. Fang, Correspondence between winding numbers and skin modes in non-Hermitian systems, Phys. Rev. Lett. **125**, 126402 (2020).

[61] K. Esaki, M. Sato, K. Hasebe, and M. Kohmoto, Edge states and topological phases in non-Hermitian systems, Phys. Rev. B **84**, 205128 (2011).

[62] M. Sato, K. Hasebe, K. Esaki, and M. Kohmoto, Time-reversal symmetry in non-Hermitian systems, Prog. Theor. Phys. **127**, 937 (2012).

[63] K. Kawabata, S. Higashikawa, Z. Gong, Y. Ashida, and M. Ueda, Topological unification of time-reversal and particle-hole symmetries in non-Hermitian physics, Nat. Commun. **10**, 297 (2019).

[64] C.-K. Chiu, J. C. Y. Teo, A. P. Schnyder, and S. Ryu, Classification of topological quantum matter with symmetries, Rev. Mod. Phys. **88**, 035005 (2016).

[65] T. Haga, M. Nakagawa, R. Hamazaki, and M. Ueda, Liouvillian skin effect: Slowing down of relaxation processes without gap closing, Phys. Rev. Lett. **127**, 070402 (2021).